Influence of Nitrogen Doping into Carbon on the Activation Barrier of ORR in Alkaline Medium: An Investigation Based on Eyring Analysis

*Rubul Das, Debittree Choudhury, Rajan Maurya, Shreya Sharma and Manoj Neergat**

Department of Energy Science and Engineering, Indian Institute of Technology Bombay, Powai, Mumbai- 400076, India

Physical Characterization

Table S1. Nitrogen content present in the C and N/C-900 samples obtained from XPS and CHN analysis

Catalyst	Atomic wt % of N	
	from XPS	from CHN
C	—	0.1
N/C-900	1.42	1.80

The nitrogen content present in the C and N/C-900 samples obtained from XPS and CHN analysis are shown in **Table S1**. The results are consistent with those previously reported in the literature.[1,2]

Background Current and *iR*-drop Correction

To eliminate the contribution of background current, the CV recorded in Ar-saturated 0.1 M KOH with same potentiodynamic parameters as that of ORR scan is subtracted from that of the O_2

saturated 0.1 M KOH. The ORR current is normalized to GCD geometrical surface area to determine the current density (mA cm^{-2}). The measured ORR current is first corrected for *iR*-drop using the values of the solution resistance (R_S) at 293–323 K (**Table S2**).

Table S2. Variation of R_S as a function of temperature in 0.1 M KOH for C, N/C-900 and Pt-black

Temperature (K)	R_S (Ω)		
	C	N/C-900	Pt-black
293	46.62±1	48.16±2	46.8±1
303	38.72±2	42.27±1	40.52±1
313	32.60±1	38.06±1	35.65±2
323	29.44±1	34.15±1	32.22±2

Estimation of Overpotential with Respect to the O_2/OH^- Equilibrium Potential at Each Temperature

The equilibrium potential for ORR and the potential of RHE shift negatively by exactly the same value with increasing temperature and their potential difference remains the same ($\Delta E = 1.229$ V).[3] The potential of RHE as a function of temperature is measured based on the "zero current zero potential approach" (**Table S3**).[4] The equilibrium potential of O_2/OH^- as a function of temperature *vs.* RHE, ($E^0_{O_2/OH^-}(T)$) is calculated using eqs S1 and S2 from the Gibbs free energy of formation of water ($\Delta G^0_{O_2/OH^-}(T)$).[5–7]

$$\Delta G^0_{O_2/OH^-}(T) = -295600 - 33.5T\ln(T) + 388.4T \text{ in J mol}^{-1} \quad \text{(S1)}$$

$$E^0_{O_2/OH^-}(T) = \frac{-\Delta G^0_{O_2/OH^-}(T)}{2F} \text{ in V} \quad \text{(S2)}$$

The overpotential ($\eta_{O_2/OH^-}(T)$) with respect to $E^0_{O_2/OH^-}(T)$ is determined from the measured potential *vs.* RHE at the respective temperature ($E_{O_2/OH^-}(T)$) (eq S3),

$$\eta_{O_2/OH^-}(T) = E_{O_2/OH^-}(T) - E^0_{O_2/OH^-}(T) \quad \text{(S3)}$$

Here, $E^0_{O_2/OH^-}(T)$ is the equilibrium potential of O_2/OH^- redox couple as a function of temperature and $\eta_{O_2/OH^-}(T)$ is the overpotential estimated at that respective temperature.

The measured electrode potential *vs.* Ag/AgCl (saturated KCl) at the respective temperature is converted to RHE scale using the following eq S4.

$$E_{O_2/OH^-}(T) = E_a + E_b + \frac{RT}{nF}\ln\frac{1}{[H^+]} \quad \text{(S4)}$$

Here E_a, E_b, *R*, *T*, *F*, *n* and [H^+] are the measured potential *vs.* Ag/AgCl (saturated KCl) at the respective temperature, the electrode potential of Ag/AgCl (saturated KCl) *vs.* RHE, gas constant, temperature, Faraday constant, the number of electrons transferred and concentration of H^+ ions, respectively.

All potentials reported in this study are converted to the RHE scale at each temperature.

Table S3. Variation of RHE electrode potential as a function of temperature *vs.* Ag/AgCl (saturated KCl) calibrated with "zero current zero potential" approach

Temperature (K)	$E_{RHE}(T)$ ***vs.*** $E_{Ag/AgCl}$ **(V) (Calibrated)**
293	−0.254±0.9
303	−0.246±0.9
313	−0.239±0.9
323	−0.231±1.0

ORR Activity of C, N/C-900 and Pt-black in 0.1 M KOH

Table S4. η_{onset} and $E_{1/2}$ for ORR on C and N/C-900 estimated at different temperatures in 0.1 M KOH

Temperature (K)	$\boldsymbol{\eta_{\text{onset}}}$ **(V)**		$\boldsymbol{E_{1/2}}$ **(V)**	
	C	**N/C-900**	**C**	**N/C-900**
293	−0.481	−0.405	0.673	0.736
303	−0.473	−0. 391	0.679	0.746
313	−0.466	−0.376	0.682	0.757
323	−0.460	−0.366	0.685	0.766

Stability of C, N/C-900 and Pt-black Catalyst Surfaces at the Experimental Temperature Range

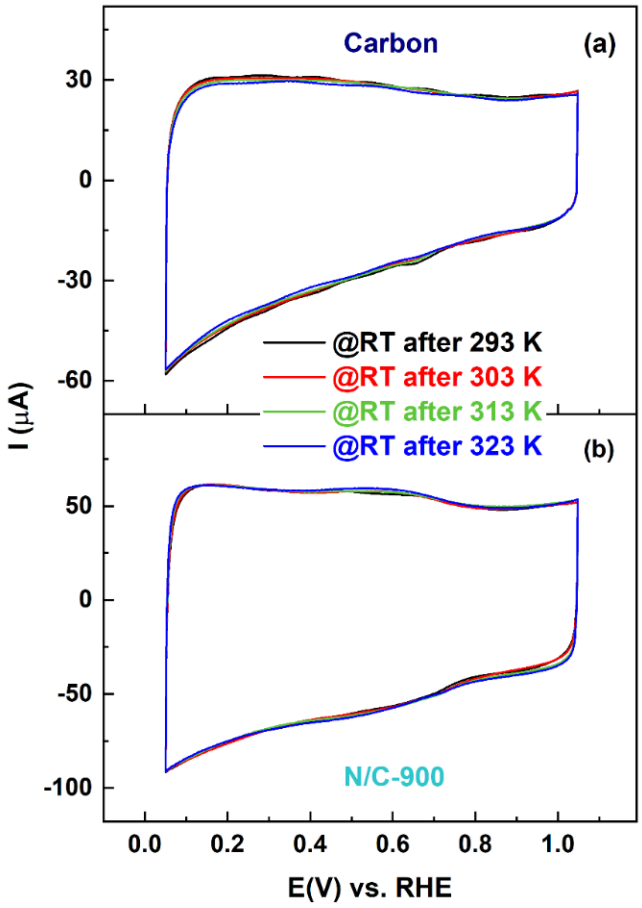

Figure S1. Voltammograms of (a) C and (b) N/C-900 in argon-saturated 0.1 M KOH at a scan rate of 50 mV s^{-1} at room temperature after the measurements were made at various temperatures.

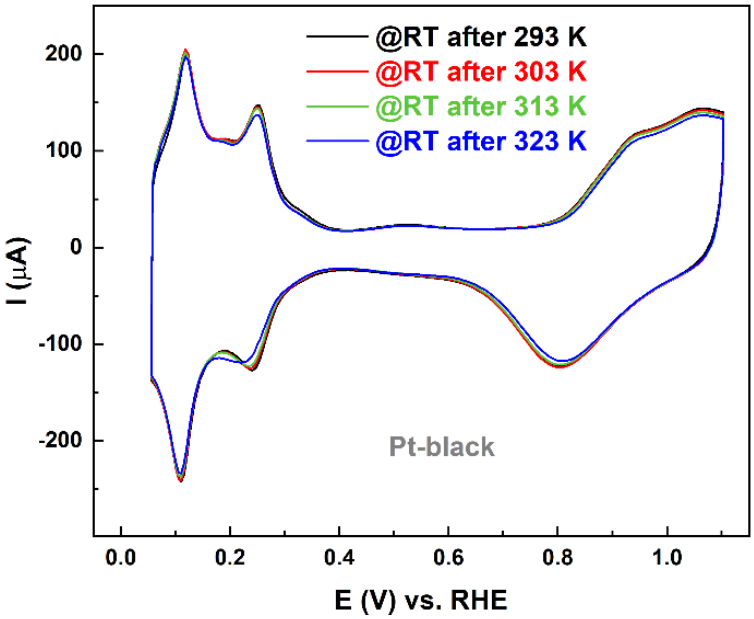

Figure S2. Voltammograms of Pt-black (51 μg cm^{-2}) in argon-saturated 0.5 H_2SO_4 at a scan rate of 50 mV s^{-1} at room temperature after the measurements were made at various temperatures.

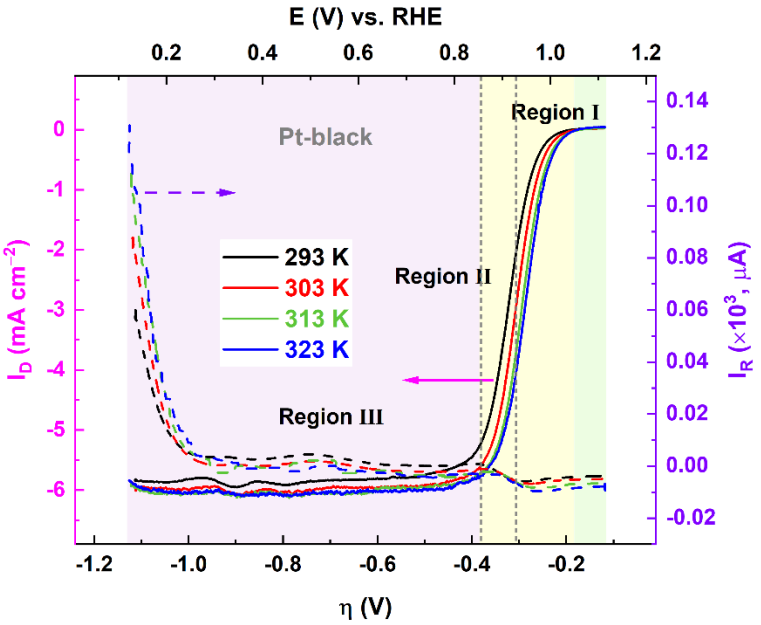

Figure S3. ORR polarization curves (solid lines) in the temperature range of 293–323 K corrected for background current and *iR*-drop on Pt-black (51 μg cm^{-2}) in oxygen-saturated 0.1 M KOH with a rotation speed of 1600 rpm at a scan rate of 10 mV s^{-1}. The dashed lines show the simultaneously recorded ring currents corresponding to HO_2^- oxidation at a ring electrode potential of 1.15 V.

Determination of Collection Efficiency (*N*)

The collection efficiency (*N*) is determined based on the reported procedures in the literature.[5] **Figure S4** shows voltammograms of 10×10^{-3} M $Fe(CN)_6^{3-}$ in argon-saturated 0.1 M NaOH recorded on Pt-black (51 μg cm^{-2}) at a scan rate of 20 mV s^{-1} with various rotation rates at 298 K. The ring electrode is potentiostated at 1.55 V, where the oxidation of $Fe(CN)_6^{4-}$to $Fe(CN)_6^{3-}$ proceeds under diffusion-control, and also oxygen evolution current at the Pt-ring is still negligible. The *N* signifies the efficiency of the ring electrode in collecting the reaction products produced at the disk electrode during the electrochemical reaction. The *N* is determined by the eq S5.

$$N = \frac{|I_{R,l}|}{|I_{D,l}|} \times 100\% \quad \text{(S5)}$$

Here, $I_{R,l}$ and $I_{D,l}$ are the ring limiting current and disk limiting current, respectively.

The calculated *N* remains constant as 25.06±0.1% at various rotation rates, as evaluated from the three independent experiments (see **Figure S5**). Also, Figure S5 shows that the *N* is independent of the rotation rate because both the anodic and cathodic limiting current is proportional to the square root of the rotation rate. The same value of *N* is also measured with the thin-film carbon and N/C-900 electrodes in the same electrode holder. Therefore, the measured *N* is used to correctly quantify the intermediate peroxide detected at the ring electrode during oxygen reduction reaction.

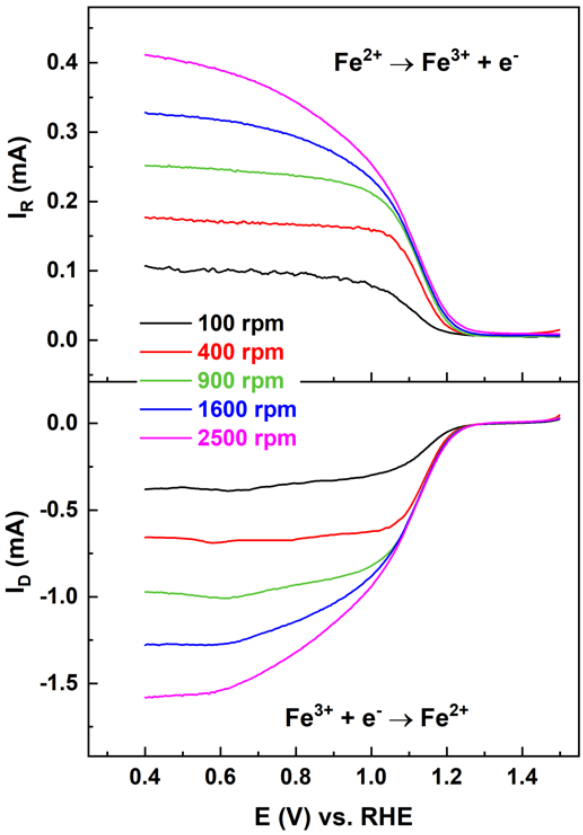

Figure S4. Voltammograms of 10×10^{-3} M $Fe(CN)_6^{3-}$ (lower panel) in argon-saturated 0.1 M NaOH on Pt-black (51 µg cm^{-2}) at a scan rate of 20 mV s^{-1} with various rotation rates at 298 K. The upper panel shows the simultaneously recorded ring currents corresponding to oxidation of $Fe(CN)_6^{4-}$ to $Fe(CN)_6^{3-}$ at a ring electrode potential of 1.55 V.

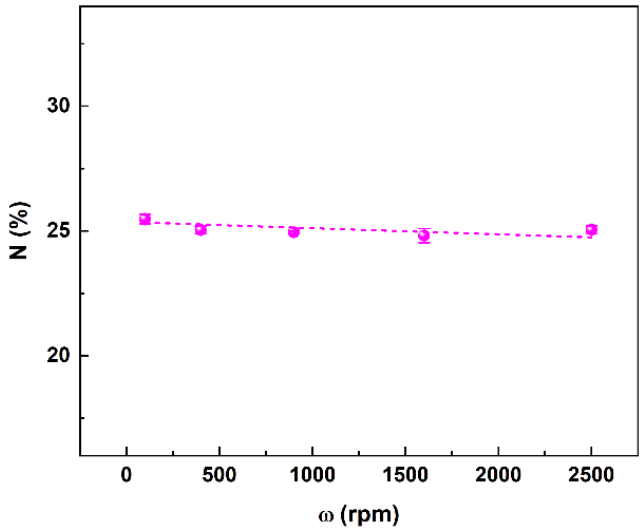

Figure S5. The calculated *N* at various rotation rates evaluated from the three independent experiments.

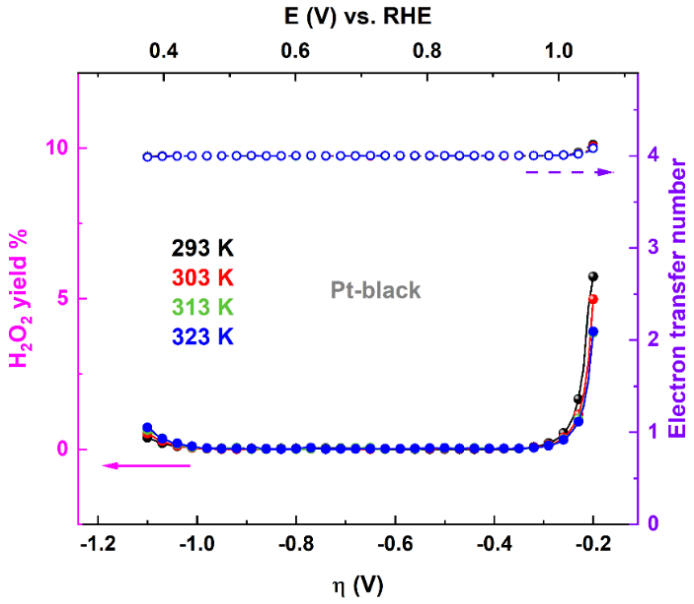

Figure S6. Percentage of HO_2^- formation (filled symbols) and average number of electron-transfer (open symbols) estimated on Pt-black during ORR in 0.1 M KOH at different temperatures.

Estimation of ORR Rate Constants (k_1, k_2, and k_3)[8–10]

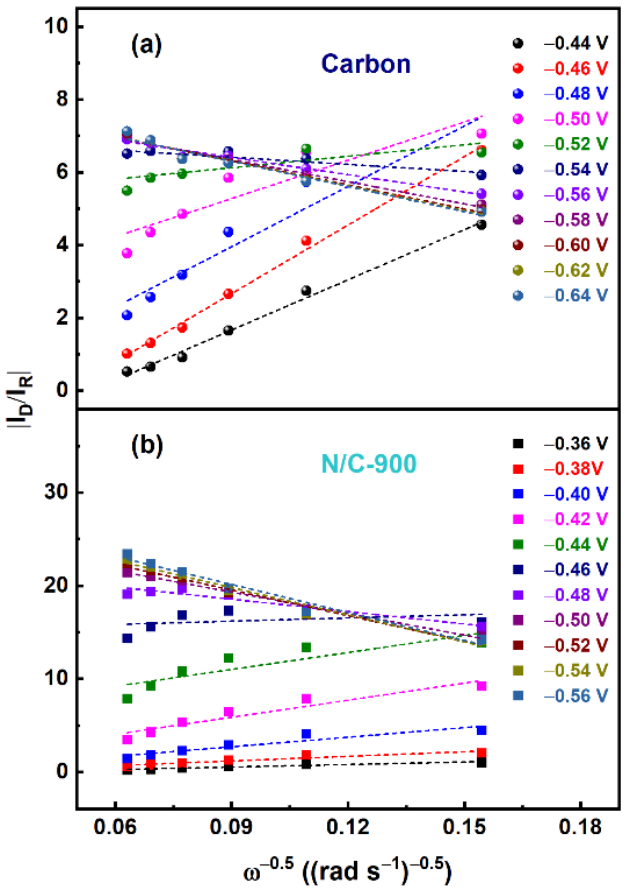

Figure S7. $\frac{I_D}{I_R}$ *vs.* $\omega^{-1/2}$ at various overpotentials for (a) C and (b) N/C-900 at room temperature.

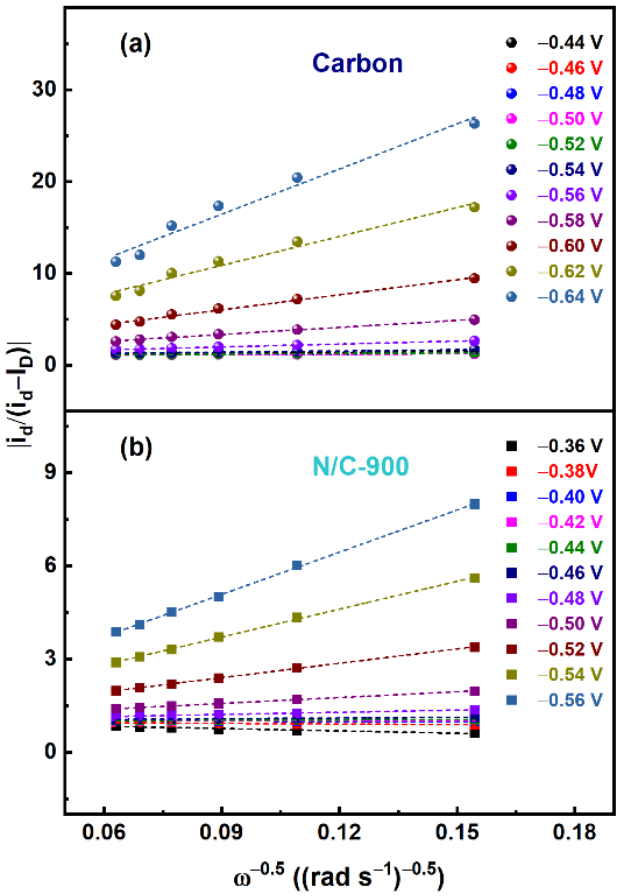

Figure S8. $\frac{i_{\mathrm{d}}}{i_{\mathrm{d}}-I_{\mathrm{D}}}$ *vs.* $\omega^{-1/2}$ at various overpotentials for (a) C and (b) N/C-900 at room temperature.

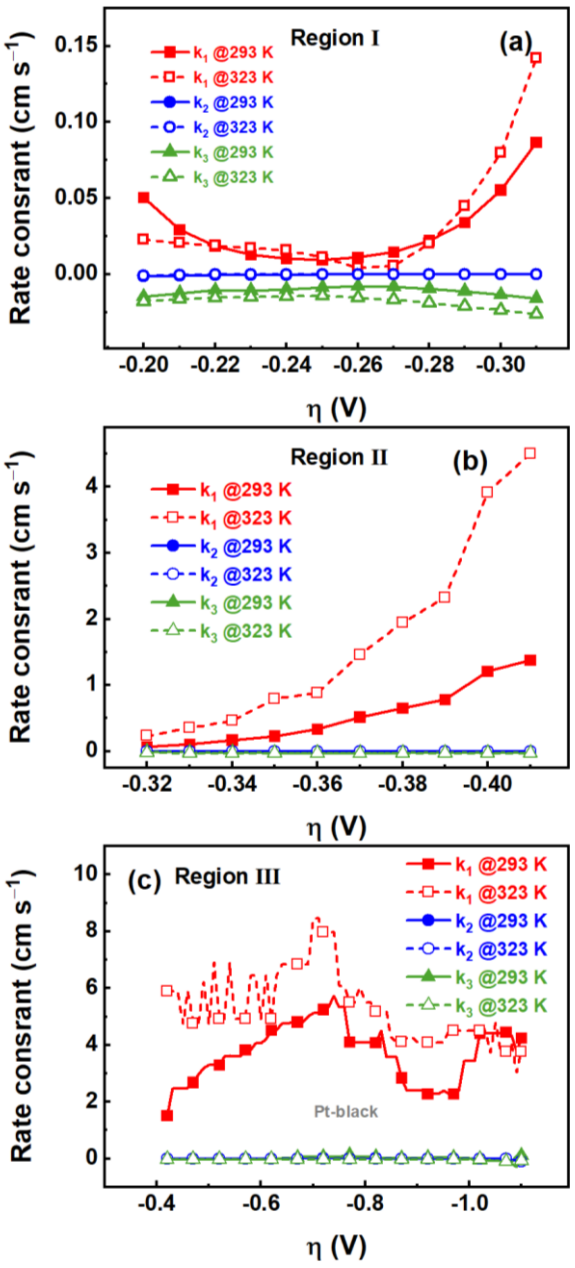

Figure S9. The individual rate constants (k_1, k_2, and k_3) for ORR in the regions I, II and III on Pt-black at 293 and 323 K.

HO_2^- Reduction on Pt-black in 0.1 M KOH

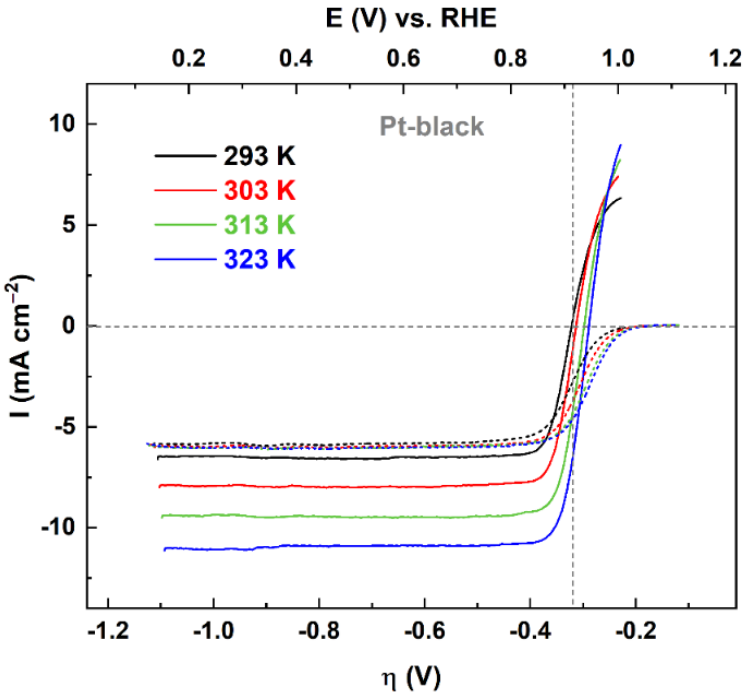

Figure S10. HO_2^- reduction polarization curves (solid lines) corrected for background current and *iR*-drop on Pt-black in argon-saturated 0.1 M KOH + 4×10^{-3} M H_2O_2 with a rotation speed of 1600 rpm at a scan rate of 10 mV s^{-1} in the temperature range of 293–323 K. The dashed lines show ORR polarization curves on the same electrode.

Estimation of Kinetic Current

The mass-transfer effects are corrected by using the Koutecky–Levich (K–L) relation (eq S6) to the ORR polarization curves corrected for background current and *iR*-drop to obtain kinetic currents (i_k).

$$\frac{1}{i} = \frac{1}{i_k} + \frac{i}{i_d} = \frac{1}{i_k} + \frac{1}{i_k}\frac{\text{func}\,(E)}{\sqrt{\omega}} \qquad \text{(S6)}$$

where i is the measured current, i_k and i_d the kinetic current and the diffusion-limited current, respectively, and ω is the rotational rate (rad s^{-1}).

The extrapolated intercept of K–L plot corresponds to the i_k (**Figure S11**).

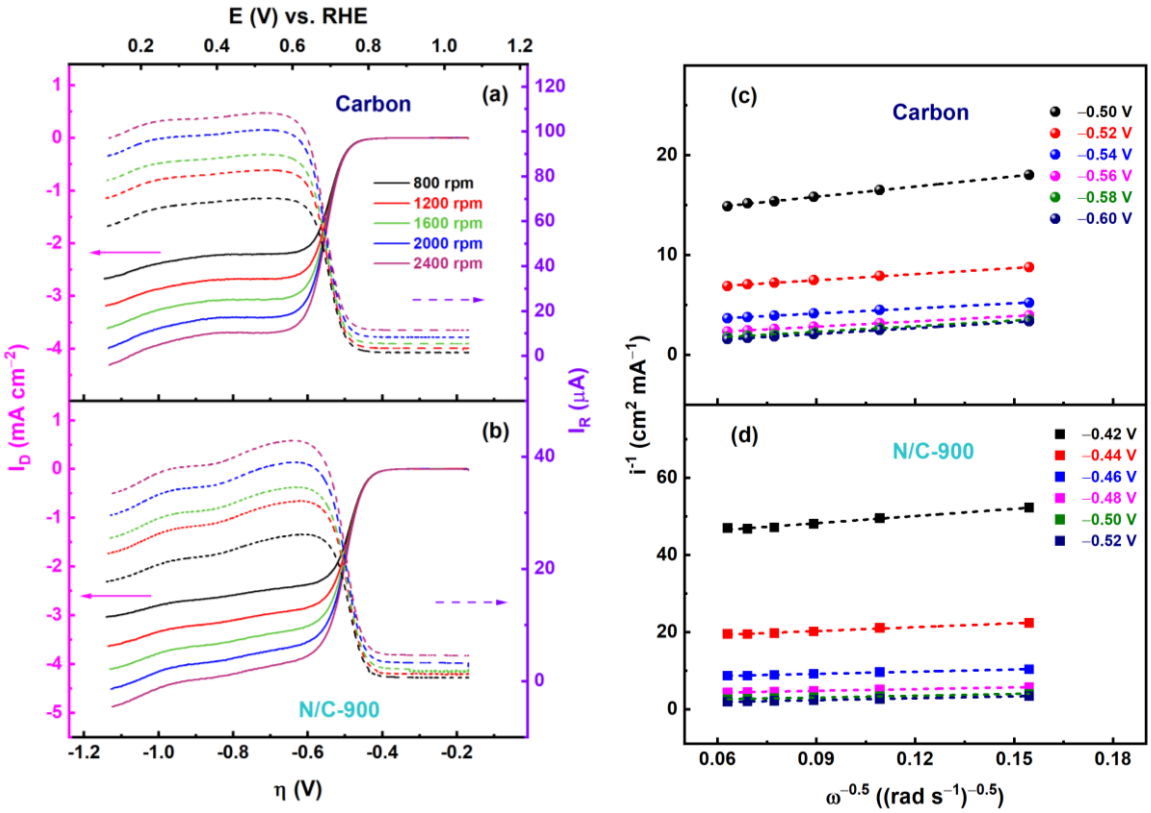

Figure S11. Background subtracted ORR polarization curves (solid lines) corrected for *iR*-drop on (a) C and (b) N/C-900 in oxygen-saturated 0.1 M KOH with various rotation speed at a scan rate of 10 mV s^{-1} at room temperature. The dashed lines show the simultaneously recorded ring current corresponding to HO_2^- oxidation at a ring electrode potential of 1.15 V. Corresponding Koutecky-Levich plot at various electrode potentials (c) C and (d) N/C-900.

The kinetic current due the reduction of O_2 to HO_2^- during ORR (i_{k,HO_2^-}) is calculated using the following eqs S7 and S8.

$$i_k = i_{k,HO_2^-} + i_{k,OH^-} \quad \text{(S7)}$$

$$i_{k,HO_2^-} = i_k \times \frac{HO_2^- (\%)}{100} \quad \text{(S8)}$$

Here, i_k is the measured kinetic current for ORR and , i_{k,OH^-} is the kinetic current due to the formation of OH^-.

However, i_{k,OH^-} is not used for the further analysis of the kinetic parameters because the amount of OH^- formed either due to direct reduction of O_2 to OH^- and/or further reduction of HO_2^- to OH^- is not quantifiable from the experimental results. On the other hand, on Pt-black a well-defined limiting current plateau is observed from the ORR polarization curves (Figure S3). Thus, the i_k for ORR is determined from the eq S6 directly. Also, the i_{k,HO_2^-} on Pt-black is considered insignificant as HO_2^- formation is negligible (~<1%).

Eyring Analysis and Estimation of Change in Enthalpy of Activation

Table S5. Summary of $\Delta H^{\#}$ for HO_2^- formation on C and N/C-900 in 0.1 M KOH at various η

Overpotential (V)	**$\Delta H^{\#}$ (kJ mol^{-1})**	
	C	**N/C-900**
−0.42	—	34.52
−0.44	—	32.11
−0.46	—	28.32
−0.48	—	22.22
−0.50	24.52	15.23
−0.52	24.17	8.93
−0.54	22.83	—
−0.56	20.91	—
−0.58	17.57	—
−0.60	15.18	—

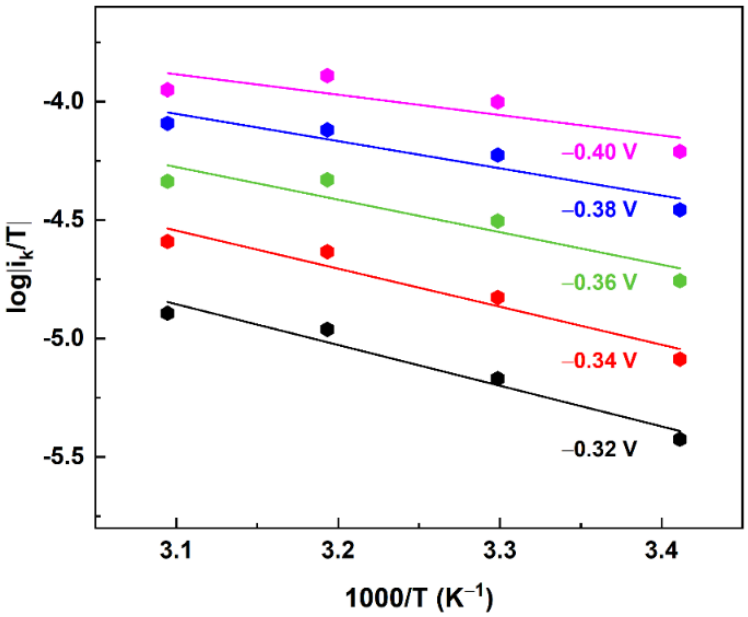

Figure S12. Eyring plots for the ORR on Pt-black at different η in the temperature range 293–323 K.

Table S6. Summary of $\Delta H^{\#}$ for ORR on Pt-black in 0.1 M KOH at various η

Overpotential (V)	**$\Delta H^{\#}$ (kJ mol^{-1})**
	Pt-black
−0.32	35.48
−0.34	33.30
−0.36	28.85
−0.38	24.54
−0.40	21.20
−0.42	19.01

Table S7. Comparison of α values derived from Eyring plots and Tafel analysis for HO_2^- formation on C and N/C-900 with temperatures

Temperature (K)	**C**		**N/C-900**	
	Eyring plots	**Tafel analysis**	**Eyring plots**	**Tafel analysis**
293	0.8	0.8	1.98	0.9
303	0.7	0.8	1.95	0.9
313	0.7	0.8	1.93	0.9
323	0.7	0.7	1.90	0.8

Tafel Analysis for HO_2^- Formation on C and N/C-900 in 0.1 M KOH at Various Temperatures

The Tafel plots for HO_2^- formation on (a) C and (b) N/C-900, following eq S9,[11] in the temperature range 293–323 K are plotted in **Figure S11**.

$$\eta = \frac{2.3RT}{\alpha F}\log|i_0| - \frac{2.3RT}{\alpha F}\log\left|i_{\mathrm{k},HO_2^-}\right| \quad \text{(S9)}$$

Here, α is the charge-transfer coefficient.

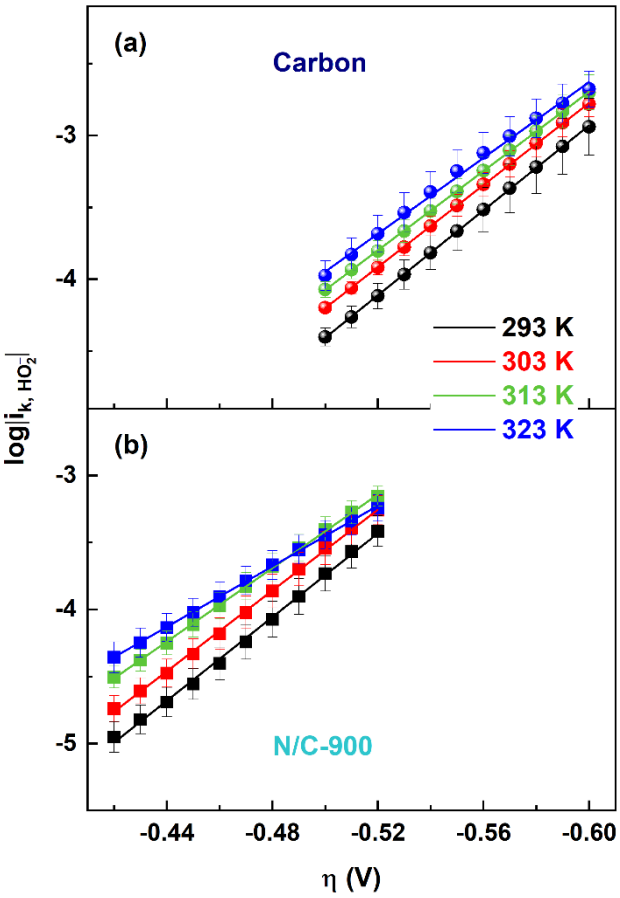

Figure S13. Tafel plots for HO_2^- formation on (a) C and (b) N/C-900 in 0.1 M KOH at different temperatures.

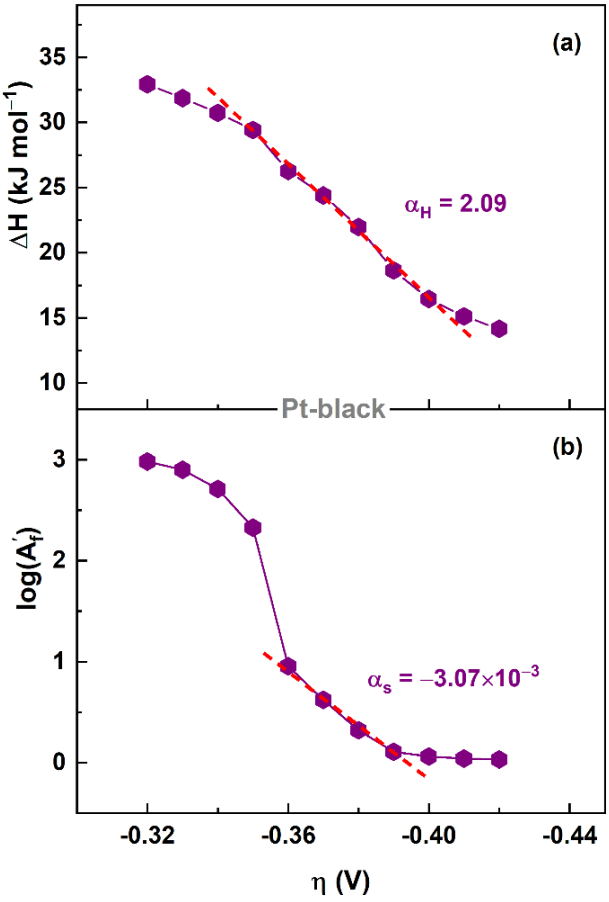

Figure S14. The trend of $\Delta H^{\#}$ (a) and $\log(A_f^{'})$ (b) with the corresponding overpotential range for ORR on Pt-black.

Tafel Analysis for ORR on Pt-black in 0.1 M KOH at Various Temperatures

Tafel slope values proportional to $\frac{2.303RT}{F}$ at low overpotential and values proportional to $\frac{2\times2.303RT}{F}$ at high overpotential are observed on Pt-black electrodes.

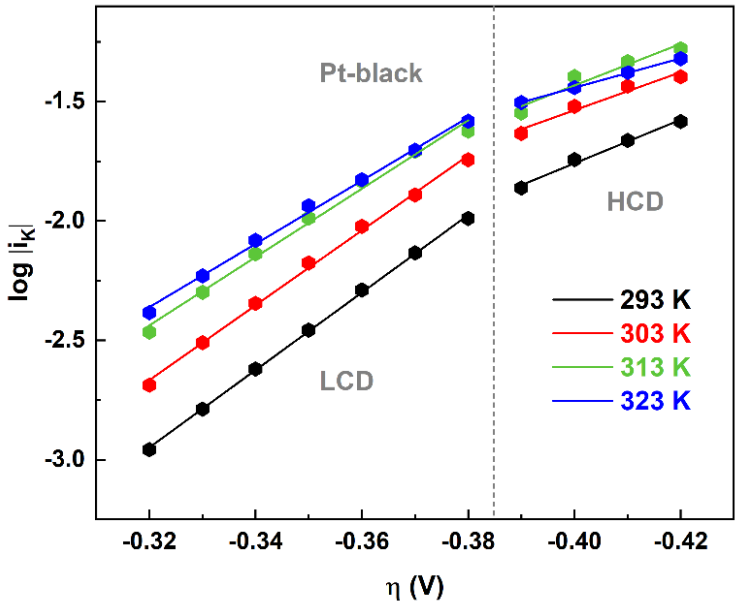

Figure S15. The trend of $\Delta H^{\#}$ (a) and $\log(A_f^{'})$ (b) with the corresponding overpotential range for ORR on Pt-black.

Table S8. Comparison of α values derived Eyring plots and Tafel analysis for ORR on Pt-black in 0.1 M KOH with temperatures

Temperature (K)	**Pt-black**	
	Eyring plots	**Tafel analysis (LCD)**
293	1.19	0.8
303	1.16	0.8
313	1.13	0.7
323	1.10	0.7

Estimation of Q_{dl} and C_{dl} of C and N/C-900 in 0.1 M KOH at Various Temperatures

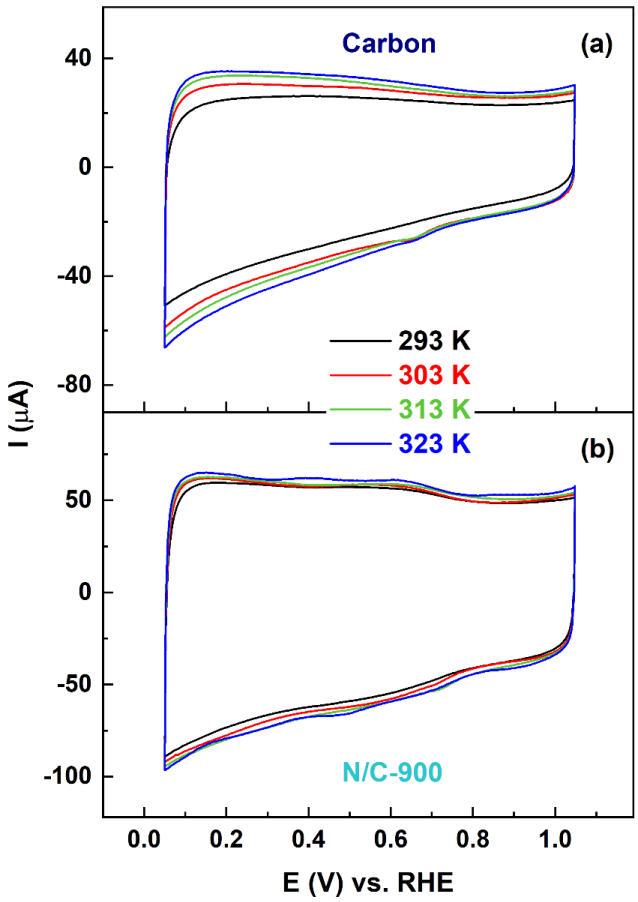

Figure S16. Voltammograms of (a) C and (b) N/C-900 in argon-saturated 0.1 M KOH at a scan rate of 50 mV s^{-1} at different temperatures.

Figure S16a and **S16**b shows the voltammograms of C and N/C-900, respectively, in the potential range of 0.05–1.05 V in argon-saturated 0.1 M KOH solution at a scan rate of 50 mV s^{-1} in the temperature range between 293–323 K. It is observed that both the catalysts show typical featureless voltammograms and no faradic processes occurs on the surfaces in the investigated potential range. The rectangular loop-shaped voltammograms indicate primarily the double-layer charging/discharging process on C and N/C-900. The double-layer charge and specific capacitance of C and N/C-900 are estimated using the eqs S10 and S11.

$$Q_{\mathrm{dl}} = \frac{\int IdV}{2 \times v} \quad \text{(S10)}$$

$$C_{\mathrm{dl}} = \frac{\int IdV}{2 \times m \times v \times (\Delta V)} \quad \text{(S11)}$$

Here, Q_{dl} is the double-layer charge (C), C_{dl} is the specific capacitance (F g^{-1}), m is the mass of electrode material (g), v is the scan rate (mV s^{-1}), ΔV is the potential range (V) and I denotes the instantaneous current on CV (A).

The Q_{dl} and C_{dl} increase with N-doping on C and it appears to be slightly temperature-dependent. The resulting Q_{dl} and C_{dl} are presented in **Table S9**. At room temperature, the higher values of Q_{dl} (1107 μC) and C_{dl} (43 F g^{-1}) of N/C-900 may be ascribed to the better surface wettability of N-containing carbon.

Table S9. Q_{dl} and C_{dl} of C and N/C-900 in 0.1 M KOH at various temperatures

Temperature (K)	**Double-layer Charge (μC)**		**Specific Capacitance (F g^{-1})**	
	C	**N/C-900**	**C**	**N/C-900**
293	487	1085	19	42
303	574	1123	22	44
313	604	1158	23	45
323	638	1207	25	46

References

1. Bera, B.; Chakraborty, A.; Kar, T.; Leuaa, P.; Neergat, M. Density of States, Carrier Concentration, and Flat Band Potential Derived from Electrochemical Impedance Measurements of N-Doped Carbon and Their Influence on Electrocatalysis of Oxygen Reduction Reaction. *J. Phys. Chem. C* **2017**, *121* (38), 20850–20856.
2. Chakraborty, A.; Devivaraprasad, R.; Bera, B.; Neergat, M. Electrochemical Estimation of the Active Site Density on Metal-Free Nitrogen-Doped Carbon Using Catechol as an Adsorbate. *Phys. Chem. Chem. Phys.* **2017**, *19* (37), 25414–25422.
3. Jerkiewicz, G. Standard and Reversible Hydrogen Electrodes: Theory, Design, Operation, and Applications. *ACS Catal.* 2020, *10* (15), 8409–8417.
4. Choudhury, D.; Das, R.; Tripathi, A. K.; Priyadarshani, D.; Neergat, M. Kinetics of Hydrogen Evolution Reactions in Acidic Media on Pt, Pd, and MoS_2. *Langmuir* **2022**, *38* (14), 4341–4350.
5. Paulus, U. A.; Schmidt, T. J.; Gasteiger, H. A.; Behm, R. J. Oxygen Reduction on a High-Surface Area Pt/Vulcan Carbon Catalyst: A Thin-Film Rotating Ring-Disk Electrode Study. *J. Electroanal. Chem.* **2001**, *495* (2), 134–145.
6. Wakabayashi, N.; Takeichi, M.; Itagaki, M.; Uchida, H.; Watanabe, M. Temperature-Dependence of Oxygen Reduction Activity at a Platinum Electrode in an Acidic Electrolyte Solution Investigated with a Channel Flow Double Electrode. *J. Electroanal. Chem.* **2005**, *574* (2), 339–346.
7. Parthasarathy, A.; Srinivasan, S.; Appleby, A. J.; Martin, C. R. Temperature Dependence of the Electrode Kinetics of Oxygen Reduction at the Platinum/Nafion® Interface—A Microelectrode Investigation. *J. Electrochem. Soc.* **1992**, *139* (9), 2530–2537.

8. Damjanovic, A.; Genshaw, M. A.; O'M Bockris, J. Distinction between Intermediates Produced in Main and Side Electrodic Reactions. *J. Chem. Phys.* **1966**, *45* (11), 4057–4059.
9. Hsueh, K. L.; Chin, D. T.; Srinivasan, S. Electrode Kinetics of Oxygen Reduction: A Theoretical and Experimental Analysis of the Rotating Ring-Disc Electrdoe Method. *J. Electroanal. Chem. Interfacial Electrochem*. **1983**, *153* (1-2), 79–95.
10. Anastasijević, N. A.; Dimitrijević, Z. M.; Adžić, R. R. Oxygen Reduction on a Ruthenium Electrode in Acid Electrolytes. *Electrochim. Acta* **1986**, *31* (9), 1125–1130.
11. Bard, A. J.; Faulkner, L. R. *Electrochemical Methods: Fundamentals and Applications*, 2nd ed.; John Wiley & Sons, 2001; pp 103−105.